Critical time-step for DEM simulations of dynamic systems using a Hertzian contact model

INTERNATIONAL JOURNAL FOR NUMERICAL METHODS IN ENGINEERING

Int. J. Numer. Meth. Engng 0000; **00**:2–33

Published online in Wiley Online Library (wileyonlinelibrary.com). DOI: 10.1002/nme

Critical time-step for DEM simulations of dynamic systems using a Hertzian contact model

Shane J. Burns[1] *, Petri T. Piiroinen [2], Kevin J. Hanley[1]

[1]*School of Engineering, Institute for Infrastructure and Environment, The University of Edinburgh, Edinburgh EH9 3JL, UK*

[2]*School of Mathematics, Statistics & Applied Mathematics, National University of Ireland Galway, University Road, Galway, Ireland*

SUMMARY

The discrete element method typically uses an explicit numerical integration scheme to solve the equations of motion. However, like all explicit schemes, the scheme is only conditionally stable, with the stability determined by the size of the time-step. Currently, there are no comprehensive techniques for estimating appropriate DEM time-steps when a nonlinear contact interaction is used. It is common practice to apply a large factor of safety to these estimates to ensure stability which unnecessarily increases the computational cost of these simulations. This work introduces an alternative framework for selecting a stable time-step for nonlinear contact laws, specifically for the Hertz–Mindlin contact law. This approach uses the fact that the discretised equations of motion take the form of a nonlinear map and can be analysed as such. Using this framework, we analyse the effects of both system damping and the initial relative velocity of collision on the critical time-step for a Hertz–Mindlin contact event between spherical particles. Copyright © 0000 John Wiley & Sons, Ltd.

Received . . .

KEY WORDS: DEM; Time-step; Stability; Hertzian contact; Damping

Prepared using nmeauth.cls *[Version: 2016/03/02 v3.01]*

1. INTRODUCTION

The discrete element method (DEM), introduced by Cundall and Strack [1], is a powerful tool used in engineering for the simulation of bulk granular materials. The particles are described using a rigid-body formulation coupled with a penalty-based interaction law. A small amount of overlap (typically $< 5\%$ of the particle radius) is allowed and from this the corresponding contact force is calculated. The impact phase is described using a combination of linear and nonlinear springs, dampers and sliders. The choice of interaction law is determined based on material behaviour, experimentation and experience.

The equations of motion for the interacting particles reduce to a system of second-order differential equations which, in almost all cases, must be solved using a numerical integration scheme. The most commonly used algorithms are the central difference, Position-Verlet and Gear's Predictor-Corrector. A detailed comparison of these time-integration methods, in terms of accuracy, stability and capability, is given by Rougier et al. [2]. The three time-integration schemes mentioned here are of second-order accuracy and can be constructed using a variable or fixed time-step Δt [3]. In this work we will consider only the constant time-step formulation in which the scheme is conditionally stable, like all explicit numerical integration techniques, based on the size of Δt [4]. Choosing too small a time-step leads to excessively long simulation times whereas an overly large time-step causes numerical instability and an unphysical solution with the possibility of energy generation [5].

The techniques being used at present to estimate suitable DEM time-steps are based on many assumptions [6], some of which lack a physical or a numerical justification and most of which are being applied to systems for which the analysis was not intended. To account for the various

*Correspondence to: School of Engineering, Institute for Infrastructure and Environment, The University of Edinburgh, Edinburgh EH9 3JL, UK. E-mail: shane.burns111@gmail.com

Contract/grant sponsor: EPSRC; contract/grant number: EP/N004477/1

Prepared using nmeauth.cls
DOI: 10.1002/nme

assumptions made in the estimation, large 'factors of safety' are applied to the calculated time-steps which in many cases leads to the adoption of conservative time-steps which slow down the simulations unnecessarily. One of the most commonly used criteria for choosing a time-step in both linear and nonlinear cases is the $\sqrt{\frac{m}{k}}$ dependency based on Belytschko [7]. This approach calculates the critical time-step as a function of the mass and stiffness of the particles in the system. This method makes use of a corollary of Rayleigh's theorem to derive the stability criterion for the discretised form of the system's equations of motion. This is achieved using modal decomposition to reduce the system to a single-degree-of-freedom system. The maximum stable time-step Δt_c is calculated for this simple system by ensuring that none of the eigenvalues of the amplification matrix have a magnitude exceeding 1 [8]. A similar approach was used in [9] in which the maximum stable time-step is calculated using the minimum particle mass and maximum particle stiffness, introducing the $\sqrt{\frac{m}{k}}$ dependency along with a safety factor. Very few studies have considered a time-step analysis for nonlinear systems: most advancements in the area have been developed for idealised linear systems only. A study by Han et al. [10] which does consider a nonlinear systems analysis involves a linearisation of the nonlinear system at each time-step in which a local limit is evaluated to determine the critical time-step. The result has the typical $\sqrt{\frac{m}{k}}$ dependency, with k, the equivalent stiffness, changing at each time increment, and m, the effective mass, held constant. Otsubo et al. [11] investigate the effect of particle mass, contact stiffness and coordination number on the critical time-step for a nonlinear contact model. Wada et al. [12] use the theoretical duration time of contact of 1-D perfectly elastic identical spherical particles as an estimate for the critical time-step. They employ a factor of safety equal to 20 to account for damping and other effects. A similar approach involves choosing the critical time-step as a fraction of the theoretical contact duration predicted by Hertz contact theory [13].

Another commonly used approach for nonlinear systems, e.g., [14, 15], involves calculating the value for the spring constant in the normal direction k_N, and using this value, together with the Belytschko $\sqrt{\frac{m}{k}}$ criterion, an estimate is made of the critical time-step. Tu and Andrade [16] propose a similar method that is based on the relative rotational motion of the contacting particles.

Prepared using nmeauth.cls
DOI: 10.1002/nme

Although this approach has its merits, it will not be reliable for most situations, and a large factor of safety will always have to be applied to ensure numerical stability. The Belytschko criterion only applies to linear systems so using the criterion for a nonlinear interaction is incorrect and cannot be justified. Another approach, discussed in section 2, is based on the Rayleigh wave velocity propagating through a static particulate system

Overall, the methods being used at present to estimate appropriate time-steps for nonlinear systems are not very reliable. As most DEM users use a nonlinear contact law for their analyses, it is very important to improve upon these techniques to enable stable, efficient simulations. The overall aim of this work is to present an alternative way for selecting stable time-steps for DEM simulations using nonlinear contact laws. For this purpose, we will derive a general framework for analysing the contact phase of the collision which takes the form of a nonlinear map. Using this map, together with various physical constraints, we will present a scheme for estimating the critical time-step.

This article is organised as follows. Section 2 describes the two most commonly used methodologies for estimating the critical time-step and further motivates the need for a new methodology. In Section 3, we will use the example of a two-sphere collision subject to a Hertzian contact law to present our methodologies for selecting a time-step. We also examine a simple linear contact interaction to verify the consistency of our general framework with previous studies. Section 4 compares our methodology with the current *state of the art* and highlights the advantages of a more reliable time-step formulation. In Section 5, we introduce the idea of dynamical systems theory and how it can be applied to the system presented in Section 3, before concluding in Section 6.

2. CURRENT METHODOLOGIES

2.1. Stability as a function of mass and stiffness

In this methodology, the critical time-step for a DEM simulation is calculated as a function of the mass m and stiffness k of the system's particles, typically giving a time-step proportional to $\sqrt{\frac{m}{k}}$.

Prepared using nmeauth.cls
DOI: 10.1002/nme

This widely used approach relies on a corollary of Rayleigh's theorem, the essential details of which we will give here.

Consider the system of second-order differential equations

$$M\ddot{q} + C\dot{q} + Kq = F, \tag{1}$$

where M, C and K are the respective mass, damping and stiffness matrices, F is the column vector of external forces and torques, and q, $\dot{q}$ and $\ddot{q}$ are the displacement, velocity and acceleration vectors, respectively. Belytschko [7] uses modal decomposition to reduce (1) to a system with a single degree of freedom and further derives the corresponding stability criterion of the reduced discretised system using spectral stability analysis. The maximum stable time-step Δt_c can be determined by calculating the eigenvalues of the amplification matrix, and is given by

$$\Delta t_c = \frac{2}{\omega_{max}} \tag{2}$$

for a linear, undamped system [17, 3, 8]. This is the approach adopted to determine time-steps in explicit finite element codes such as LS-DYNA [18] and ABAQUS/Explicit [19], even for nonlinear problems. The inclusion of damping reduces the maximum time-step in both of these finite element codes to

$$\Delta t_c = \frac{2}{\omega_{max}} \left(\sqrt{1 + \zeta^2} - \zeta \right) \tag{3}$$

where ζ is a damping ratio. Belytschko [7] gives the following relation

$$\omega_{max} = \sqrt{\lambda_{max}}, \tag{4}$$

where λ_{max} is the maximum eigenvalue of $M^{-1}K$. Equation (4) is derived using an extension of Rayleigh's bounding theorem [7], which relates the eigenvalues of any two systems which are equivalent apart from linear constraints. Applied to a particulate system simulated using DEM, this approach invariably leads to $\Delta t_c \propto \sqrt{\frac{m}{k}}$.

A shortcoming of this analysis is that it requires the modal equations of motion to decouple. This necessitates the imposition of certain restrictions on the damping matrix C which are often unphysical. The method developed in [7] assumes Rayleigh damping: C is defined as a linear

Prepared using nmeauth.cls
DOI: 10.1002/nme

combination of the mass and stiffness matrices. An additional major shortcoming is that this analysis only applies to systems that are linear with respect to the generalised coordinates. As most DEM formulations use a nonlinear contact interaction model, using a linear analysis may yield a highly inaccurate stability bound.

2.2. Stability using the Rayleigh time-step

The second commonly used methodology is based on the principle that energy cannot propagate from a particle beyond its adjacent neighbouring particles in a single time-step [20]. The assumption is made that all energy transferred across a particulate system is due to Rayleigh waves and the contributions of distortional and dilational waves, collectively accounting for around one-third of radiated energy [21], can therefore be neglected. The critical time-step is calculated using the theoretical expression for the Rayleigh wave velocity for a system such that

$$\Delta t_c = \frac{\pi r}{\beta}\sqrt{\frac{\rho}{G}}, \tag{5}$$

where r is the particle radius, ρ is the particle density, G is the shear modulus and β can be approximated by [20, 22]

$$\beta = 0.8766 + 0.163\nu, \tag{6}$$

where ν is the Poisson's ratio of the particle.

Even for this relatively simple approach, there is some ambiguity about the particle radius to be used in (5) for a polydisperse size distribution. The radius of the smallest particle in the system, r_{min}, is used by [23, 24] whereas [20, 22] instead use the average particle radius, $\bar{r}$, in (5). For monosized particles, $\bar{r} = r_{\text{min}}$, but as the degree of polydispersity in the system increases, Δt_c calculated using r_{min} becomes increasingly more conservative than the form of (5) including $\bar{r}$.

The Rayleigh time-step criterion has been used for decades,see e.g. [22], and its continued popularity implies that its use generally leads to stable simulations. However, this may not be the case for highly dynamic systems. It is known that time-steps should be reduced when particle relative velocities are high [25] but the Rayleigh approach lacks any velocity dependence, as can be

Prepared using nmeauth.cls
DOI: 10.1002/nme

seen from the form of (5). Furthermore, the Rayleigh time-step does not consider system damping. Thus the critical time-step calculated for the static assembly may be orders of magnitude larger than would be required to ensure numerical stability for a highly dynamic, damped case.

Both of these existing methodologies, the two most popular among DEM users, have major deficiencies for dynamic simulations with damping. This is currently addressed by applying large factors of safety to the critical time-steps calculated using either methodology, leading to inefficient simulations. This motivates the need to develop an alternative way to select time-steps for dynamical systems with nonlinear contact interactions.

3. TWO-PARTICLE COLLISION

In this section, we will present the general mathematical framework for a two-sphere collision which is compatible with any contact model. We consider the two-particle collision of H and H' with masses m and m', radii r and r' and moments of inertia I and I', as shown in Figure 1. The displacement and rotation of the centre of mass G of body H can be described in the frame located at G by the coordinates q_1, q_2 and q_3 and the angular rotation θ_1, θ_2 and θ_3 and similarly q_1', q_2' and q_3' are the coordinates and θ_1', θ_2' and θ_3' are the rotations of the centre of mass G' of body H'. We let

$$q = (q_1, q_2, q_3, \theta_1, \theta_2, \theta_3)^T, \quad q' = (q_1', q_2', q_3', \theta_1', \theta_2', \theta_3')^T,$$

$$\dot{q} = (\dot{q}_1, \dot{q}_2, \dot{q}_3, \dot{\theta}_1, \dot{\theta}_2, \dot{\theta}_3)^T, \quad \dot{q}' = (\dot{q}_1', \dot{q}_2', \dot{q}_3', \dot{\theta}_1', \dot{\theta}_2', \dot{\theta}_3')^T,$$

be the displacement and velocity vectors of the centre of mass of H and H', respectively. We define F and F' as the forces generated at impact of each body given by

$$F = (-F_1, -F_2, -F_3) \quad \text{and} \quad F' = (F_1, F_2, F_3)\,,$$

where the subscripts 1 or 3 represent the components of position, velocity and the contact force acting in the tangent plane, and the subscript 2 denotes the components acting in the direction normal to the tangent plane. The direction in which the force due to gravity acts does not affect the derivation; here it is arbitrarily assumed to act in the direction normal to the tangent plane with

Prepared using nmeauth.cls
DOI: 10.1002/nme

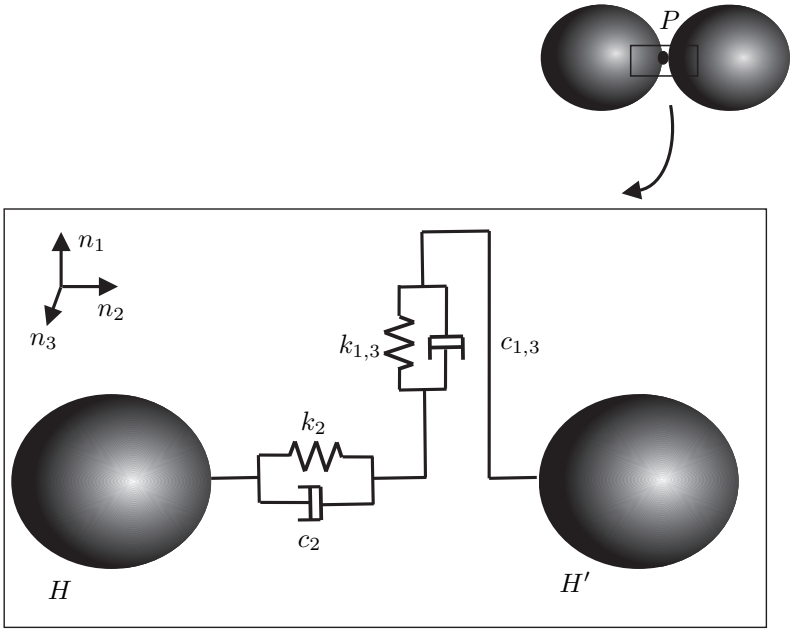

Figure 1. Simplified 2D view of a collinear impact between two spheres H and H' with radii r and r' separated in the normal direction by a Hertzian spring with spring constant k_2, and separated in the tangential directions by linear springs with spring constants k_1 and k_3, respectively. Linear damping acts in all directions with constants c_1, c_2 and c_3. The initial relative velocity between the two bodies at impact is denoted by v_i.

gravitational acceleration g. This is the only external force or torque acting on H or H'. Using Newton's second law, the equations of motion for sphere H and sphere H' at contact can be found such that

$$\frac{d\dot{q}_1}{dt} = -\frac{F_1}{m}, \tag{7}$$

$$\frac{d\dot{q}_2}{dt} = -\frac{F_2}{m} - g, \tag{8}$$

$$\frac{d\dot{q}_3}{dt} = -\frac{F_3}{m}, \tag{9}$$

$$\frac{d\dot{\theta}_1}{dt} = -\frac{rF_3}{I}, \tag{10}$$

$$\frac{d\dot{\theta}_2}{dt} = 0, \tag{11}$$

$$\frac{d\dot{\theta}_3}{dt} = \frac{rF_1}{I}. \tag{12}$$

Prepared using nmeauth.cls
DOI: 10.1002/nme

Similarly, the equations of motion for sphere H' are given by

$$\frac{d\dot{q'}_1}{dt} = \frac{F_1}{m'}, \tag{13}$$

$$\frac{d\dot{q'}_2}{dt} = \frac{F_2}{m'} - g, \tag{14}$$

$$\frac{d\dot{q'}_3}{dt} = \frac{F_3}{m'}, \tag{15}$$

$$\frac{d\dot{\theta'}_1}{dt} = -\frac{r'F_3}{I'}, \tag{16}$$

$$\frac{d\dot{\theta'}_2}{dt} = 0, \tag{17}$$

$$\frac{d\dot{\theta'}_3}{dt} = \frac{r'F_1}{I'}. \tag{18}$$

3.1. Reducing the dimension of the system

For analysis purposes we are only interested in the dynamics that occur during the contact phase. It is intuitive therefore to consider the system given by (7) – (18) in terms of a relative frame located at the contact point of each sphere. We define the position q_P of the contact point P of sphere H relative to the $n_1 - n_2 - n_3$ frame as

$$q_P := (q_{1P}, q_{2P}, q_{3P})^T, \tag{19}$$

where

$$q_{1P} = q_1 - r\theta_3, \quad q_{2P} = q_2, \quad q_{3P} = q_3 + r\theta_1 \tag{20}$$

and where

$$\dot{q}_{1P} = \dot{q}_1 - r\dot{\theta}_3, \quad \dot{q}_{2P} = \dot{q}_2, \quad \dot{q}_{3P} = \dot{q}_3 + r\dot{\theta}_1. \tag{21}$$

Similarly, for sphere H' we have that

$$q'_P := (q'_{1P}, q'_{2P}, q'_{3P})^T, \tag{22}$$

where

$$q'_{1P} = q'_1 + r'\theta'_3, \quad q'_{2P} = q'_2, \quad q'_{3P} = q'_3 - r'\theta'_1 \tag{23}$$

and where

$$\dot{q'}_{1P} = \dot{q'}_1 + r'\dot{\theta'}_3, \quad \dot{q'}_{2P} = \dot{q'}_2, \quad \dot{q'}_{3P} = \dot{q'}_3 - r'\dot{\theta'}_1. \tag{24}$$

Prepared using nmeauth.cls
DOI: 10.1002/nme

The differential equations for the changes in velocity at the contact point P of particle H can be ascertained by evaluating

$$\frac{d\dot{q}_{1P}}{dt} = \frac{d\dot{q}_{1P}}{d\dot{q}_1}\frac{d\dot{q}_1}{dt} + \frac{d\dot{q}_{1P}}{d\dot{\theta}_3}\frac{d\dot{\theta}_3}{dt}, \tag{25}$$

$$\frac{d\dot{q}_{2P}}{dt} = \frac{d\dot{q}_{2P}}{d\dot{q}_2}\frac{d\dot{q}_2}{dt}, \tag{26}$$

$$\frac{d\dot{q}_{3P}}{dt} = \frac{d\dot{q}_{3P}}{d\dot{q}_3}\frac{d\dot{q}_3}{dt} + \frac{d\dot{q}_{3P}}{d\dot{\theta}_1}\frac{d\dot{\theta}_1}{dt}. \tag{27}$$

Using (7) – (12) together with (21) and (25) – (27) we have that

$$\begin{pmatrix} \ddot{q}_{1P} \\ \ddot{q}_{2P} \\ \ddot{q}_{3P} \end{pmatrix} = \begin{pmatrix} -\frac{1}{m} - \frac{r^2}{I} & 0 & 0 \\ 0 & -\frac{1}{m} & 0 \\ 0 & 0 & -\frac{1}{m} - \frac{r^2}{I} \end{pmatrix} \begin{pmatrix} F_1 \\ F_2 \\ F_3 \end{pmatrix} + \begin{pmatrix} 0 \\ -g \\ 0 \end{pmatrix}, \tag{28}$$

and similarly, for H' we have that

$$\begin{pmatrix} \ddot{q'}_{1P} \\ \ddot{q'}_{2P} \\ \ddot{q'}_{3P} \end{pmatrix} = \begin{pmatrix} \frac{1}{m'} + \frac{r'^2}{I'} & 0 & 0 \\ 0 & \frac{1}{m'} & 0 \\ 0 & 0 & \frac{1}{m'} + \frac{r'^2}{I'} \end{pmatrix} \begin{pmatrix} F_1 \\ F_2 \\ F_3 \end{pmatrix} + \begin{pmatrix} 0 \\ -g \\ 0 \end{pmatrix}. \tag{29}$$

Now that we have translated the frame of reference to the contact point of each sphere, we can further simplify by considering relative velocity changes at the common point of contact. For this purpose we let

$$\tilde{q_1} = q_{1P} - {q'}_{1P}, \quad \tilde{q_2} = q_{2P} - {q'}_{2P} + (r' + r), \quad \tilde{q_3} = q_{3P} - {q'}_{3P}. \tag{30}$$

Using (28), (29) and (30) gives

$$\begin{pmatrix} \ddot{\tilde{q}}_1 \\ \ddot{\tilde{q}}_2 \\ \ddot{\tilde{q}}_3 \end{pmatrix} = \begin{pmatrix} -\frac{1}{m} - \frac{r^2}{I} - \frac{1}{m'} - \frac{r'^2}{I'} & 0 & 0 \\ 0 & -\frac{1}{m} - \frac{1}{m'} & 0 \\ 0 & 0 & -\frac{1}{m} - \frac{r^2}{I} - \frac{1}{m'} - \frac{r'^2}{I'} \end{pmatrix} \begin{pmatrix} F_1 \\ F_2 \\ F_3 \end{pmatrix}, \tag{31}$$

which is the change in the relative contact point velocity for H and H'. We can further simplify by using the fact that $I = \frac{2}{5}mr^2$ and $I' = \frac{2}{5}m'r'^2$ and defining the reduced mass $\hat{m} = \frac{mm'}{m+m'}$ to give

$$\begin{pmatrix} \ddot{\tilde{q}}_1 \\ \ddot{\tilde{q}}_2 \\ \ddot{\tilde{q}}_3 \end{pmatrix} = \begin{pmatrix} -\frac{7}{2\hat{m}} & 0 & 0 \\ 0 & -\frac{1}{\hat{m}} & 0 \\ 0 & 0 & -\frac{7}{2\hat{m}} \end{pmatrix} \begin{pmatrix} F_1 \\ F_2 \\ F_3 \end{pmatrix}, \tag{32}$$

Prepared using nmeauth.cls
DOI: 10.1002/nme

which is the relative acceleration of the contact point of the contacting spheres during the impact phase. This reduced system will make subsequent analysis much simpler.

3.2. 1-D Undamped Linear Contact

To illustrate the usability of this technique, we first consider a trivial, linear, undamped contact interaction with forcing in the normal direction only. The contact force F now takes the form

$$F = \begin{pmatrix} 0 \\ k_2 \tilde{q}_2 \\ 0 \end{pmatrix}, \tag{33}$$

where k_2 represents the normal contact spring stiffness. Substituting (33) into (32) gives the following system of equations

$$\begin{pmatrix} \ddot{\tilde{q}}_1 \\ \ddot{\tilde{q}}_2 \\ \ddot{\tilde{q}}_3 \end{pmatrix} = \begin{pmatrix} 0 & 0 & 0 \\ 0 & -\frac{k_2}{\hat{m}} & 0 \\ 0 & 0 & 0 \end{pmatrix} \begin{pmatrix} \tilde{q}_1 \\ \tilde{q}_2 \\ \tilde{q}_3 \end{pmatrix}. \tag{34}$$

The maximum stable time-step Δt_c can then be calculated using the methodology in section 2.1 and using (2), (4) and (34) to give

$$\Delta t_c = 2\sqrt{\frac{\hat{m}}{k_2}}. \tag{35}$$

Substituting $m' = m$ into (35), to allow for a direct comparison with the system considered in [17], gives

$$\Delta t_c = \sqrt{2}\sqrt{\frac{m}{k_2}}, \tag{36}$$

which is identical to the bound reported in [17].

3.3. Hertz–Mindlin Contact

We now consider a nonlinear contact law and use this to illustrate the methods we are proposing for choosing a stable time-step. Specifically we consider the Hertz–Mindlin contact law together with

Prepared using nmeauth.cls
DOI: 10.1002/nme

linear damping as stated below, such that

$$F_1 = c_1\dot{\tilde{q}}_1 + k_1\tilde{q}_2{}^{\frac{1}{2}}\tilde{q}_1, \tag{37}$$

$$F_2 = c_2\dot{\tilde{q}}_2 + k_2\tilde{q}_2{}^{\frac{3}{2}}, \tag{38}$$

$$F_3 = c_3\dot{\tilde{q}}_3 + k_3\tilde{q}_2{}^{\frac{1}{2}}\tilde{q}_3, \tag{39}$$

where c_1, c_3 and c_2 are the equivalent damping constants in the shear directions and normal direction respectively and where k_1, k_3 and k_2 are the equivalent spring constants in the same directions. Equations (37) – (39) are then used, together with (32), to form the equations of motion for a Hertz–Mindlin contact interaction. The next step is to discretise the system using the commonly used central difference algorithm.

3.4. Discretised solution

For a detailed description of the Verlet-type central difference algorithm used in this paper, for both fixed and variable time-steps, the reader is referred to [2]. For this analysis, we will consider an interval of time $[0, T]$ partitioned into n discrete instances of time given by $t_n = n\Delta t$. We also introduce the half instances of time such that the velocities at the half instances are given by

$$\dot{\tilde{q}}_{j\,n-\frac{1}{2}} = \frac{x_{j\,n} - x_{j\,n-1}}{\Delta t}, \quad \dot{\tilde{q}}_{j\,n+\frac{1}{2}} = \frac{x_{j\,n+1} - x_{j\,n}}{\Delta t}. \tag{40}$$

Then, the second derivative term is given by

$$\ddot{\tilde{q}}_{j\,n} = \frac{\dot{\tilde{q}}_{j\,n+\frac{1}{2}} - \dot{\tilde{q}}_{j\,n-\frac{1}{2}}}{\Delta t}, \tag{41}$$

and the discretised form of (32) can be written as

$$\ddot{q_1}_n = -\frac{7}{2\hat{m}}k_1 {x_2}_n{}^{\frac{1}{2}} {x_1}_n - \frac{7}{2\hat{m}}c_1\dot{\tilde{q}}_{1\,n-\frac{1}{2}}, \tag{42}$$

$$\ddot{q_2}_n = -\frac{k_2}{\hat{m}}{x_2}_n{}^{\frac{3}{2}} - \frac{c_2}{\hat{m}}\dot{\tilde{q}}_{2\,n-\frac{1}{2}}, \tag{43}$$

$$\ddot{q_3}_n = -\frac{7}{2\hat{m}}k_3 {x_2}_n{}^{\frac{1}{2}} {x_3}_n - \frac{7}{2\hat{m}}c_3\dot{\tilde{q}}_{3\,n-\frac{1}{2}}, \tag{44}$$

For clarity, we will introduce a new notation to eliminate the half time instances. For this purpose we let $\hat{v}_n := \dot{\tilde{q}}_{n-\frac{1}{2}}$ which gives the following system:

Prepared using nmeauth.cls DOI: 10.1002/nme

$$\hat{v_1}_{n+1} = \hat{v_1}_n - \Delta t \left(\frac{7}{2\hat{m}} k_1 {x_2}_n^{\frac{1}{2}} x_{1n} + \frac{7}{2\hat{m}} c_1 \hat{v_1}_n \right), \tag{45}$$

$$x_{1n+1} = x_{1n} + \Delta t \hat{v_1}_{n+1}, \tag{46}$$

$$\hat{v_2}_{n+1} = \hat{v_2}_n - \Delta t \left(\frac{k_2}{\hat{m}} {x_2}_n^{\frac{3}{2}} + \frac{c_2}{\hat{m}} \hat{v_2}_n \right), \tag{47}$$

$$x_{2n+1} = x_{2n} + \Delta t \hat{v_2}_{n+1}, \tag{48}$$

$$\hat{v_3}_{n+1} = \hat{v_3}_n - \Delta t \left(\frac{7}{2\hat{m}} k_3 {x_2}_n^{\frac{1}{2}} x_{3n} + \frac{7}{2\hat{m}} c_3 \hat{v_3}_n \right), \tag{49}$$

$$x_{3n+1} = x_{3n} + \Delta t \hat{v_3}_{n+1}. \tag{50}$$

The original complex dynamics described by (7) – (18) has been greatly reduced to the system (45) – (50). In Section 3.6, we will use this equivalent system to determine bounds on the time-step. Before this discussion, it is necessary to distinguish between numerical stability and accuracy for this nonlinear problem.

3.5. *Stability* vs. *accuracy*

While it is well known that the numerical stability of a DEM simulation depends on the chosen simulation time-step, so too does the accuracy of the simulation. For a contact between two Hertzian spheres using the second-order velocity-Verlet integration scheme, Hanley and O'Sullivan [26] show that, during a single calculation cycle, the truncation error in an energy balance is a function of particle radii, density, shear modulus, Poisson's ratio, simulation time-step and the relative velocity between colliding particles. The magnitude of this truncation error generally increases with the last two of these factors, i.e., by increasing the time-step or relative velocity, both of which move a simulation closer to instability, the truncation error increases.

Despite this apparent similarity, there is a clear difference between the concepts of accuracy and stability. The accrued error in an energy balance will be small for a stable simulation; the signs of error terms during loading and unloading differ, giving a total error of zero for the perfectly symmetrical load reversal discussed in [26]. Instability is characterised by an uncontrolled, non-physical growth of energy in a simulation [5], which may be easily detected using an energy balance.

Prepared using nmeauth.cls
DOI: 10.1002/nme

In Section 3.6, we identify two significant analytical curves which may be drawn on a plot of relative velocity against inter-particle overlap. It is proposed that a stable time-step should be small enough so that these two analytical curves are not crossed in one time-step: at least one time-step is needed to describe the first phase of the impact between initial contact and maximum compression, and at least one time-step to describe the second phase between maximum compression and minimum relative velocity. If this condition were not met, it would be possible for collision events to be missed entirely.

It is instructive to consider the analogue of Section 3.2 for an undamped Hertzian contact. The Hertzian analogues of Equations (33) and (34) are

$$F = \begin{pmatrix} 0 \\ k_2 \tilde{q}_2{}^{\frac{3}{2}} \\ 0 \end{pmatrix} \tag{51}$$

and

$$\begin{pmatrix} \ddot{\tilde{q}}_1 \\ \ddot{\tilde{q}}_2 \\ \ddot{\tilde{q}}_3 \end{pmatrix} = \begin{pmatrix} 0 & 0 & 0 \\ 0 & -\frac{k_2 \tilde{q}_2{}^{\frac{1}{2}}}{\hat{m}} & 0 \\ 0 & 0 & 0 \end{pmatrix} \begin{pmatrix} \tilde{q}_1 \\ \tilde{q}_2 \\ \tilde{q}_3 \end{pmatrix}, \tag{52}$$

where the $\tilde{q}_2{}^{\frac{1}{2}}$ term represents the square root of inter-particle overlap. If this term is taken to be fixed for the purposes of this illustration, so that this linear analysis can be applied, then

$$\Delta t_c \approx \sqrt{\frac{2m}{k_2 \tilde{q}_2{}^{\frac{1}{2}}}} \tag{53}$$

for identical spheres of mass m. The smallest possible Δt_c arises from choosing the largest overlap. The maximum overlap between identical Hertzian spheres of radius r, $\tilde{q}_{2\max}$, is given as [13, 27]

$$\tilde{q}_{2\max} = r \left(\frac{5\sqrt{2}\pi\rho}{4} \frac{1-\nu^2}{E} {v_{2i}}^2 \right)^{\frac{2}{5}}, \tag{54}$$

in which the Young's modulus $E = 2G(1+\nu)$. Equation (54) can be substituted into (53) to obtain an expression for Δt_c as a function of v_{2i} if this linear analysis is assumed to be applicable (an assumption which is not required in Section 3.6). The expression thus obtained is approximately

Prepared using nmeauth.cls
DOI: 10.1002/nme

$0.6t_H$, where t_H is the duration of a Hertzian contact between identical spheres [13, 27]:

$$t_H = 2.94\left(\frac{5\sqrt{2}\pi\rho}{4}\frac{1-\nu^2}{E}\right)^{\frac{2}{5}}\frac{r}{{v_{2i}}^{\frac{1}{5}}}. \tag{55}$$

Thus, this linear analysis based on Rayleigh's bounding theorem [7] approximates a critical Hertzian time-step a little larger than half of the contact duration, i.e., 1–2 time-steps are required at a minimum to describe a two-particle contact. This matches the required minimum number of time-steps for stability in the analysis presented in Section 3.6. As the simulation time-step is reduced more and more below the critical value needed for numerical stability, the accuracy of the simulation will progressively improve [26].

3.6. Analysis of the impact phase

In this section, we will present the main results of this work and give our motivation for selecting a time-step in this manner. Our techniques involve analysing the impact phase, using the framework derived in Sections 3.1 – 3.4, and deriving meaningful bounds based on the physics of the collision. A note on linear stability theory is presented in Section 5. This will enable comparison with the bounds derived in this section without linearisation of the system. It will be demonstrated in Section 5 that linear stability theory is unable to describe these complex nonlinear interactions and is therefore not a suitable basis for choosing a time-step; this explains why (53) which is based on a linear assumption is only presented as an illustrative approximation.

3.6.1. Normal direction First let us consider the normal direction. We define the following

$$\hat{V} := \hat{v_{2_{n+1}}} - \hat{v_{2_n}} \tag{56}$$

$$\hat{X} := x_{2n+1} - x_{2n} \tag{57}$$

and, using (47) and (48), find the two curves $\hat{V} = 0$ and $\hat{X} = 0$. Consider firstly $\hat{X} = 0$. Here we are following the theory given in [28], where the point of maximum compression is found by solving for the instant of zero relative velocity to give

$$\hat{X} = 0 \Rightarrow \hat{v_{2_n}} = \frac{\frac{\Delta t k_2}{\hat{m}}{x_{2_n}}^{\frac{3}{2}}}{1-\frac{\Delta t c_2}{\hat{m}}}. \tag{58}$$

Prepared using nmeauth.cls
DOI: 10.1002/nme

The curve given by (58) corresponds to the point of maximum compression for a given Δt. If we consider the limit as Δt approaches zero we have that

$$\lim_{\Delta t\to 0} \hat{v_{2n}} = \lim_{\Delta t\to 0} \frac{\frac{\Delta t k_2}{\hat{m}} x_{2n}{}^{\frac{3}{2}}}{1-\frac{\Delta t c_2}{\hat{m}}} = 0, \tag{59}$$

which corresponds to the true solution for the curve of maximum compression. The solution $\hat{v_{2n}} = 0$ is expected due to the theory of [28]. As we take a smaller and smaller time-step, we approach the true value $\hat{v_{2n}} = 0$. We propose that in the first instance of motion (Phase 1), the trajectory should not cross this curve in one time-step. Considering now $\hat{V} = 0$ yields

$$\hat{V} = 0 \Rightarrow \hat{v_{2n}} = \frac{-k_2}{c_2} x_{2n}{}^{\frac{3}{2}}, \tag{60}$$

which corresponds to the point of minimum velocity, or when the restitution phase of the collision ends. At the point $\hat{V} = 0$, the two bodies go from the point of maximum compression to the point of minimal relative velocity. We propose that in the second instance of motion (Phase 2), the trajectory should not cross this curve in one time-step. In what follows, we will give a formal description of each of the two phases of motion, and determine constraint equations on the time-step Δt.

Phase 1: In the first phase of the motion the system goes from initial contact to maximum compression. Using (47) and (48) subject to the boundary conditions

$$\hat{v_{2n+1}} \approx 0 \implies x_{2n+1} \approx x_{2n} \approx \Delta t v_i, \hat{v_{2n}} \approx v_{2i} \tag{61}$$

gives

$$\left(1-\frac{\Delta t c_2}{\hat{m}}\right) - \frac{v_{2i}{}^{\frac{1}{2}} k_2}{\hat{m}} \Delta t^{\frac{5}{2}} = 0. \tag{62}$$

Equation (62) describes the dynamics of going from the initial instant of contact to the point of maximum compression. To physically capture the full impact phase it is necessary therefore to choose a time-step such that the full dynamics of the compression phase can be captured. At the least, we require one time-step to describe this phase so (62) can be solved numerically to give an upper bound on the time-step.

It is noted that increasing v_{2i} requires a smaller value of Δt to satisfy (62) with fixed values of c_2, k_2 and $\hat{m}$. It has been known for a long time that time-steps must be decreased when particle

Prepared using nmeauth.cls
DOI: 10.1002/nme

velocities, or strain rates, are high to maintain stability for the Hertzian contact model and to ensure acceptable accuracy of the simulation, e.g., the default safety factor on time-step in the PFC3D code is recommended to be reduced 'especially under rapidly changing conditions' [25]. This research quantifies the effect of v_{2_i} on time-step.

Phase 2: In the second phase the system goes from maximum compression to the point at which the relative velocity is a minimum. Using (47) subject to the following boundary conditions

$$\hat{v_{2n+1}} \approx \frac{-k_2}{c_2} {x_{2n+1}}^{\frac{3}{2}}, \hat{v_{2n}} \approx 0 \tag{63}$$

gives

$$\frac{\Delta t}{\hat{m}} \left(k_2 {x_{2n}}^{\frac{3}{2}} \right) = \frac{x_{2n+1} - x_{2n}}{\Delta t} = \frac{-k_2}{c_2} {x_{2n+1}}^{\frac{3}{2}}, \tag{64}$$

and thus

$$\Delta t_c = \left(\frac{x_{2n+1}}{x_{2n}} \right)^{\frac{3}{2}} \frac{\hat{m}}{c_2}. \tag{65}$$

During Phase 2, $x_{2n+1} < x_{2n}$ so $\Delta t_c < \frac{\hat{m}}{c_2}$ based on (65). To aid in the visualisation of this methodology, consider the schematic detailed in Figure 2 of a two-sphere collision subject to a Hertz–Mindlin contact interaction. As derived in the previous section, we consider the dynamics in terms of the relative frame located at the contact point of the spheres. The spheres come into contact with an initial positive relative velocity and leave with a negative relative velocity. Our techniques are concerned with the rich dynamics which occur throughout the contact phase, as shown in Figure 2. For each of the three initial conditions, we see that the point of maximum compression and the point of minimum velocity always occurs at the intersection of the trajectories with the theoretical curves given by (58) and (60), respectively. This allows us to choose a time-step such that we can not cross either of the two analytical curves in one time-step. The premise of this approach is that the impact phase for any collision will be fully captured and will lead to physical, stable simulations. In the absence of damping, the points of maximum compression and minimum velocity respectively coincide with $\hat{v_n} = 0$ and $x_{2n} \leq 0$.

Prepared using nmeauth.cls
DOI: 10.1002/nme

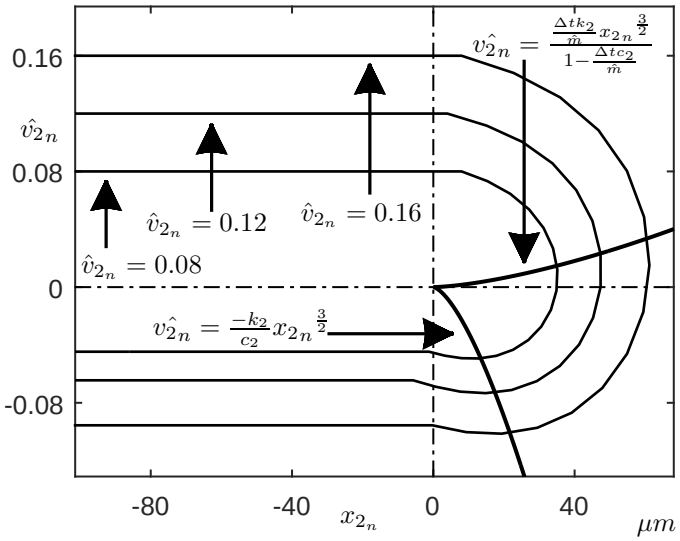

Figure 2. Relative velocity of a two-sphere collision as a function of the inter-particle overlap. Three different incident velocities are shown as contours together with the analytical expressions for the maximum overlap curve and minimum velocity curve. The spheres start with an initial positive relative velocity.

3.6.2. No slip condition (Shear bounds) In the normal direction, the stable time-step identified ensures that a velocity reversal cannot occur within one time-step after collision, i.e., the positive incident velocities on Figure 2 cannot become negative within one time-step as this would entail crossing the 'maximum overlap' curve. A similar shear bound is proposed, that the tangential velocity cannot be brought to zero in only one time-step. If, across one time-step, the shear force were sufficient to bring the tangential velocity to zero, we would achieve a velocity reversal and would likely introduce energy artificially into the system due to instability. Using (45) and (49) subject to the initial conditions

$$\hat{v_{1}}_{n+1} \approx 0 \implies x_{1\,n+1} \approx x_{1\,n} \approx \Delta t v_{1i}, x_{2n} \approx \Delta t v_{2i}, \tag{66}$$

$$\hat{v_{3}}_{n+1} \approx 0 \implies x_{3\,n+1} \approx x_{3n} \approx \Delta t v_{3i}, \hat{v_{1}}_{n} = v_{1i}, \hat{v_{3}}_{n} = v_{3i} \tag{67}$$

gives

$$1 - \frac{7}{2\hat{m}} \Delta t c_1 - \frac{7}{2\hat{m}} {v_{2i}}^{\frac{1}{2}} k_1 \Delta t^{\frac{5}{2}} = 0 \tag{68}$$

and

$$1 - \frac{7}{2\hat{m}} \Delta t c_3 - \frac{7}{2\hat{m}} {v_{2i}}^{\frac{1}{2}} k_3 \Delta t^{\frac{5}{2}} = 0. \tag{69}$$

Prepared using nmeauth.cls
DOI: 10.1002/nme

Equations (68) and (69) cannot be solved analytically but can be solved numerically to give upper bounds on the time-step.

3.6.3. Implementation For the numerical analysis that will be presented in Section 4.2.2, the critical time-step is chosen as the minimum of (62), (65), (68) and (69). In practice, a safety factor should be included to ensure the time-step chosen is not exactly at the upper bound.

3.6.4. Undamped For the undamped system, the compression and restitution phases of impact are symmetric. We therefore only need to consider one phase in the calculation of the critical time-step in the normal direction. Using (62) subject to $c_2 = 0$ gives

$$\Delta t_{c2} = \left(\frac{\hat{m}}{k_2 {v_{2_i}}^{\frac{1}{2}}} \right)^{\frac{2}{5}}. \tag{70}$$

These normal bounds have the same form as the bounds used in [12]. Considering the undamped case for the shear bounds, and using (68) and (69) subject to $c_1 = c_3 = 0$, gives

$$\Delta t_{c1} = \left(\frac{2\hat{m}}{7k_1 {v_{2_i}}^{\frac{1}{2}}} \right)^{\frac{2}{5}} \tag{71}$$

and

$$\Delta t_{c3} = \left(\frac{2\hat{m}}{7k_3 {v_{2_i}}^{\frac{1}{2}}} \right)^{\frac{2}{5}}. \tag{72}$$

Comparing (71) and (72) with (70) we see that

$$\Delta t_{c2} > \Delta t_{c1,3}, \tag{73}$$

provided $k_{1,3} > \frac{2}{7}k_2$ which is always the case referring to Section 4.1, i.e., the shear bounds dictate the critical time-step. Tu and Andrade [16] similarly found, albeit using a completely different approach, that the critical time-step is dictated by the tangential spring constants for an undamped system.

Prepared using nmeauth.cls
DOI: 10.1002/nme

4. RESULTS

4.1. *Comparison with Rayleigh time-step and Hertz contact time*

The Rayleigh time-step criterion (Section 2.2) estimates the critical time-step in terms of the particle density, shear modulus and Poisson's ratio. In order to compare our estimate for the critical time-step, it is first necessary to rewrite in terms of the same material parameters. For this purpose, we can relate the particle spring constants, controlling the contact stiffness, to the shear modulus and Poisson's ratio as follows:

$$k_{1,3} = \frac{4G\sqrt{\hat{r}}}{(2-\nu)}, \quad k_2 = \frac{4G\sqrt{\hat{r}}}{3\,(1-\nu)} \tag{74}$$

where $\hat{r} = \frac{rr'}{r+r'}$ is the reduced particle radius. Taking the ratio,

$$\frac{k_{1,3}}{k_2} = \frac{3(1-\nu)}{(2-\nu)}. \tag{75}$$

At $\nu = 0.5, k_{1,3} = k_2$; otherwise, $k_{1,3} > k_2$ for physically realistic values of ν. For the undamped system, using (70) and (74) we get

$$\Delta t_{c2} = {v_{2}}_i^{-\frac{1}{5}}\,(1-\nu)^{2/5}\left(\frac{\frac{r^3 r'^3}{r^3+r'^3}}{\sqrt{\hat{r}}}\right)^{\frac{2}{5}}\left(\frac{\pi\rho}{G}\right)^{\frac{2}{5}} \tag{76}$$

for the normal bounds. Considering the undamped case for the shear bounds, and using (68) and (69) together with (74) , gives

$$\Delta t_{c1,3} = {v_{2}}_i^{-\frac{1}{5}}\,(2-\nu)^{2/5}\left(\frac{\frac{r^3 r'^3}{r^3+r'^3}}{\sqrt{\hat{r}}}\right)^{\frac{2}{5}}\left(\frac{2\pi\rho}{21G}\right)^{\frac{2}{5}}. \tag{77}$$

Recalling the Rayleigh time-step criterion from Section 2.2, we have

$$\Delta t_c = \frac{\pi r_{\text{min}}}{0.8766 + 0.163\nu}\sqrt{\frac{\rho}{G}}, \tag{78}$$

taking the more conservative form of the criterion based on r_{min} rather than $\bar{r}$. If $r = r'$, $\Delta t_c \propto r$ in (76) and (77): the same proportionality to radius as in (78).

The duration of a Hertzian contact between identical spheres, t_H, was presented above as (55). Comparing t_H and (76), both equations have the same dependence on ν, ρ, G, r and ${v_{2}}_i$. In fact, Δt_{c2} for the undamped system is exactly half of t_H: the expected result considering the origin of (76) in Section 3.6.

Prepared using nmeauth.cls
DOI: 10.1002/nme

4.2. Numerics

In this section, we will numerically analyse how the critical time-step calculated in Section 3 is affected by the system parameters. The purpose of this is to gain insight into how damping, together with the initial relative velocity of collision, affects the critical time-step. For the undamped case, we will compare the results with the time-step predicted using the Rayleigh approach (78). For the numerical analysis in this section, we consider variants of two sets of parameters, as detailed in the figure captions.

4.2.1. Undamped Figure 3 shows the variation of critical time-step with initial relative velocity, v_i, for different contours of shear modulus when damping is inactive. At low velocities, approaching quasi-static conditions, Δt_c is greater than the Rayleigh time-step and thus less conservative. Δt_c decreases with increasing v_i. This is consistent with the recommendation within the commercial PFC3D code [25] to reduce the default value of the safety factor by which the estimated critical time-step is multiplied when the Hertzian contact model is used under rapidly changing conditions. The dashed lines in Figure 3 and all subsequent figures indicate the corresponding Rayleigh time-steps given by (78). In Figure 3, these are constant with respect to v_i. This is a major shortcoming of the Rayleigh time-step methodology as it fails to capture the known dependence of time-step on velocity. For a different set of input parameters corresponding to glass ballotini (beads), Figure 4 shows that for low velocity Δt_c is again greater than the Rayleigh time-step and thus less conservative. However, as the relative velocity increases, Δt_c becomes lower than the Rayleigh prediction.

In Figures 5 and 6, we investigate the effect of particle size on Δt_c. For this purpose, the ratio $\frac{m'}{m}$ is varied between 0 and 1 ($m \geq m'$). In both figures, Δt_c approaches zero as $\frac{m'}{m}$ approaches zero, consistent with analytical and numerical studies, e.g., [11]. As for the monosized particles, increasing v_i has the effect of decreasing Δt_c. For the industrial powder, the Rayleigh time-step is between a relative velocity of $0.1\,\mathrm{m\,s^{-1}}$ and $1\,\mathrm{m\,s^{-1}}$, whereas it is closest to $1\,\mathrm{m\,s^{-1}}$ for the glass ballotini in Figure 6. At higher velocities, e.g., during shot peening using glass beads as an abrasive

Prepared using nmeauth.cls
DOI: 10.1002/nme

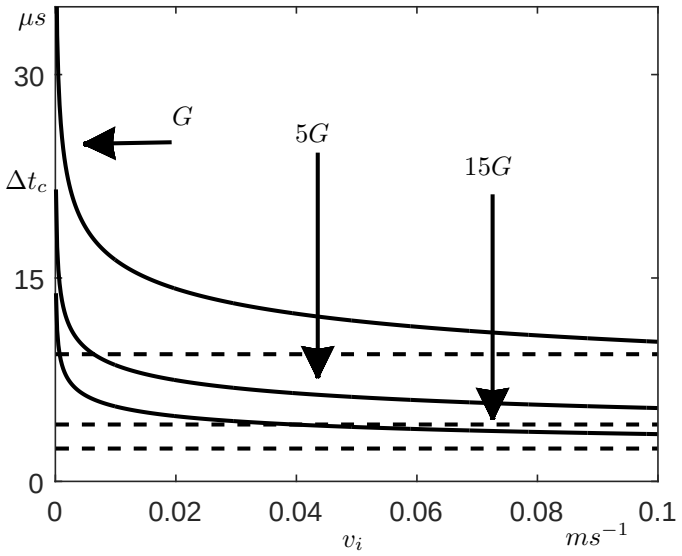

Figure 3. Critical time-step, Δt_c (solid line), against initial relative velocity, v_i. Parameters are based on those in [29] for an unspecified representative industrial powder in a simulated mixer: $G = 300\,\mathrm{MPa}$, $\nu = 0.25$, $\rho = 1000\,\mathrm{kg\,m^{-3}}$, $r = r' = 1.5\,\mathrm{mm}$. The dashed line shows the corresponding Rayleigh critical time-step.

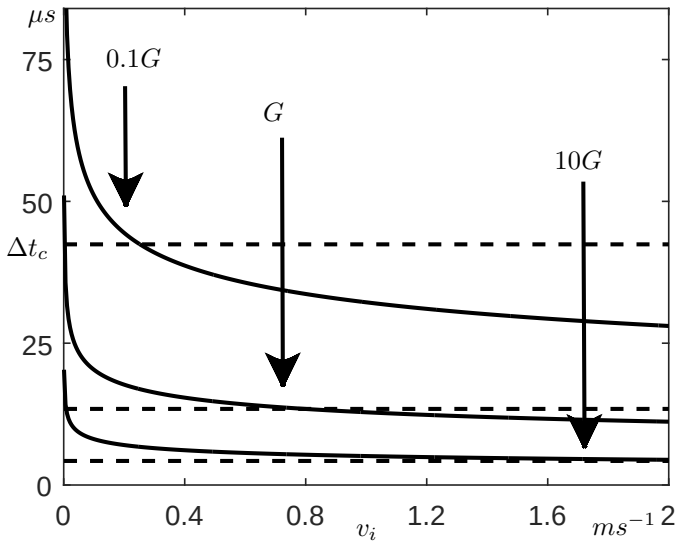

Figure 4. Critical time-step, Δt_c, against initial relative velocity, v_i using parameters for large glass ballotini from [30]: $G = 17\,\mathrm{GPa}$, $\nu = 0.22$, $\rho = 2530\,\mathrm{kg\,m^{-3}}$, $r = 10.1\,\mathrm{mm}, r' = 10.3\,\mathrm{mm}$.

DOI: 10.1002/nme

medium, choosing the Rayleigh time-step is likely to lead to instability. Conversely, the Rayleigh time-step would be unnecessarily conservative for quasi-static simulations.

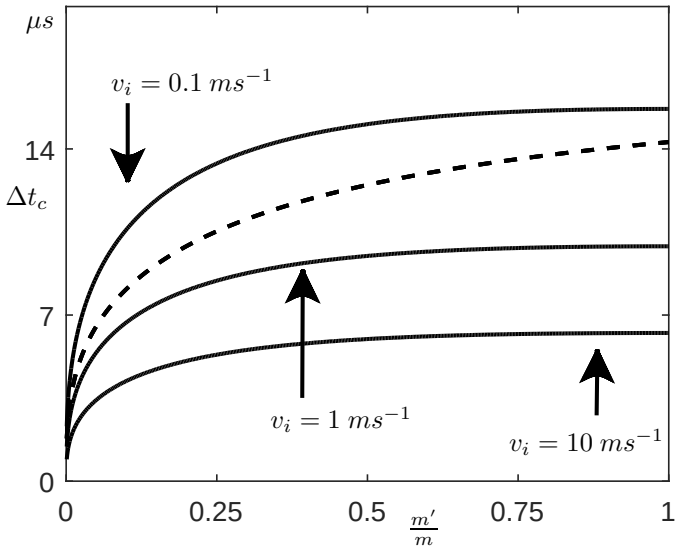

Figure 5. Critical time-step, Δt_c, against particle mass ratio, $\frac{m'}{m}$, using the values of G, ν and ρ for an industrial powder from Figure 3 and $m + m' = 0.0001$ kg.

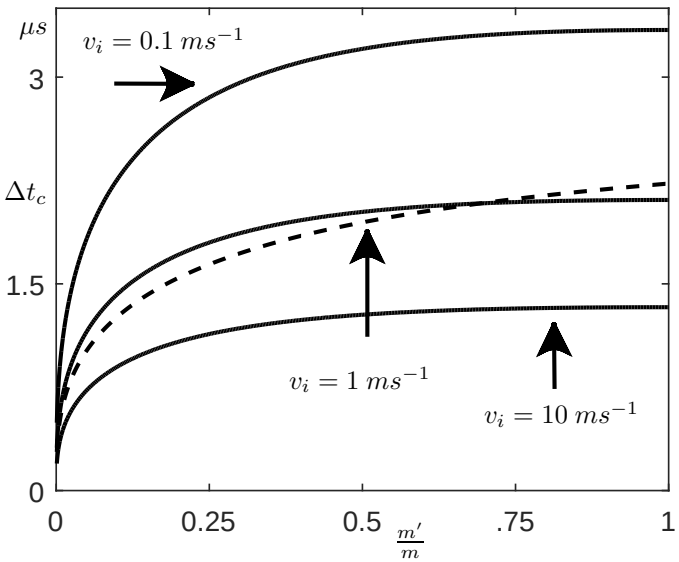

Figure 6. Critical time-step, Δt_c, against particle mass ratio, $\frac{m'}{m}$, using the values of G, ν and ρ for glass ballotini from Figure 4 and $m + m' = 0.0001$ kg.

Prepared using nmeauth.cls
DOI: 10.1002/nme

In Figures 7 and 8, we investigate the effect of particle size on Δt_c by increasing the system mass, $m + m'$, by a factor of 100 compared to those in Figures 5 and 6. The greater system mass, or particle radii considering the fixed density, has the effect of increasing Δt_c, consistent with prior studies [11]. However, the ratios between the Rayleigh time-step and the time-steps calculated using this approach are unchanged.

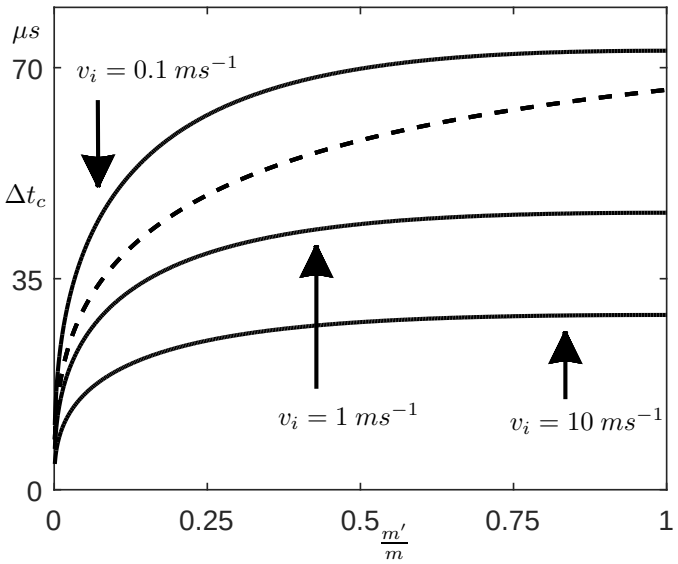

Figure 7. Critical time-step, Δt_c, against particle mass ratio, $\frac{m'}{m}$, for an industrial powder [29] with $G = 300\,\mathrm{MPa}$, $\nu = 0.25$, $\rho = 1000\,\mathrm{kg\,m^{-3}}$, $m + m' = 0.01\,\mathrm{kg}$.

4.2.2. Damped The inclusion of damping can have a very significant effect on the time-step. Invariably, the inclusion of damping necessitates a smaller time-step to ensure stability compared to the equivalent undamped case. This is an important consideration as many practical simulations contain some mechanical damping to dissipate energy. Figures 9 and 10 are for the same cases as in Section 4.2.1: a typical industrial powder and large glass beads, respectively. However, the contours now show different values of the damping constants, $c_1 = c_2 = c_3$. In both cases, for sufficiently small damping and low relative velocity, Δt_c is less conservative than the Rayleigh time-step. However, increasing c_2 beyond a certain point results in a more conservative estimate of Δt_c than predicted by Rayleigh. The Rayleigh time-step remains constant with respect to both

Prepared using nmeauth.cls
DOI: 10.1002/nme

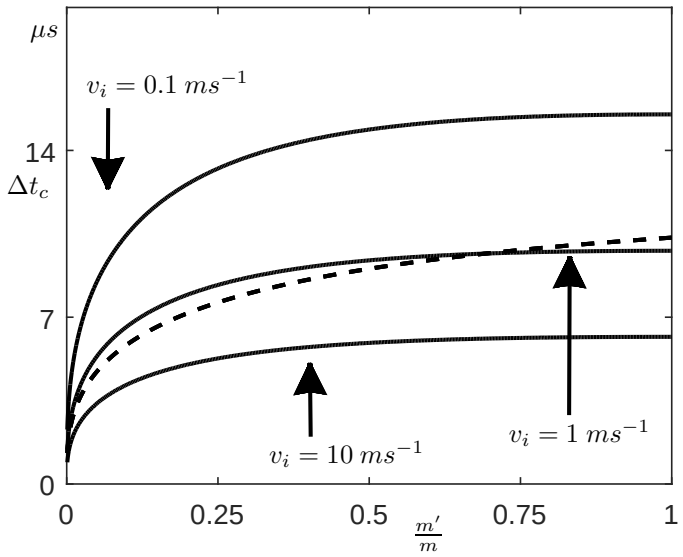

Figure 8. Critical time-step, Δt_c, against particle mass ratio, $\frac{m'}{m}$, for glass ballotini [30] with $G = 17\,\mathrm{GPa}$, $\nu = 0.22$, $\rho = 2530\,\mathrm{kg\,m^{-3}}$, $m + m' = 0.01\,\mathrm{kg}$.

c_2 and v_i, making its use as a stable bound highly unreliable when considering damped, dynamic interactions.

This result, that the inclusion of damping reduces the critical time-step, is in agreement with [31]. In that paper, a Hertz–Mindlin contact model is adopted and the damping term originates from the presence of liquid bridges between the particles. Using a semi-empirical approach, Washino et al. [31] find that the time-step must decrease to maintain stability with increasing liquid viscosity, i.e., an increasing degree of damping. Damping also reduces Δt_c in finite element codes, as seen by comparing (2) and (3).

In Figures 11 and 12, we investigate the effect of particle size on Δt_c by decreasing the ratio $\frac{m'}{m}$ for varying contours of c_2. In Figure 11, Δt_c is more conservative than the Rayleigh time-step for all c_2 due to the interaction of system parameters. However, in Figure 12, Δt_c is less conservative than the Rayleigh time-step for sufficiently low values of c_2 and $\frac{m'}{m}$.

Prepared using nmeauth.cls
DOI: 10.1002/nme

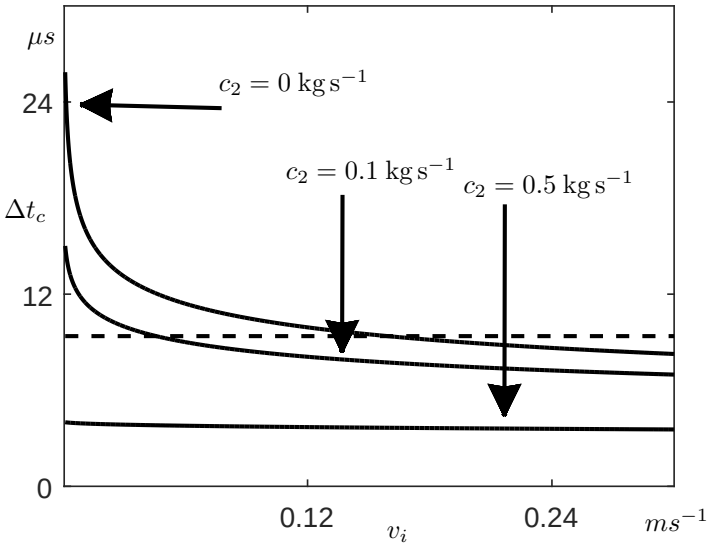

Figure 9. Critical time-step, Δt_c, against initial relative velocity, v_i, using the parameters from Figure 3 with damping constants of 0, 0.1 and 0.5 $\mathrm{kg\,s^{-1}}$ and $c_1 = c_2 = c_3$.

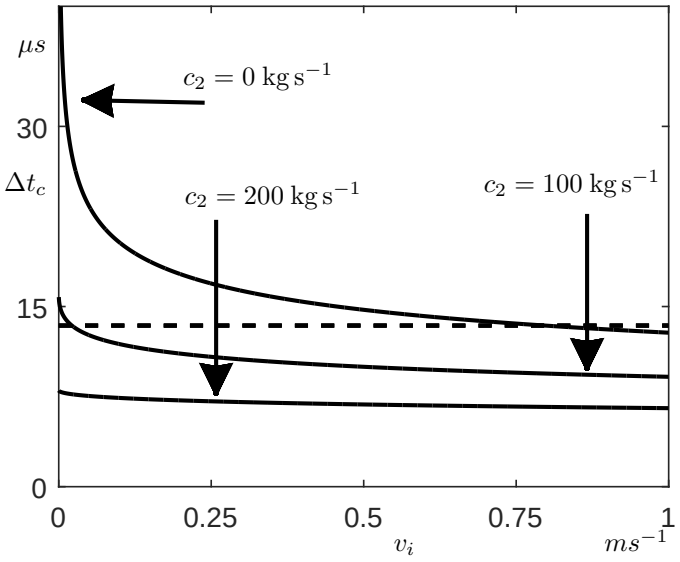

Figure 10. Critical time-step, Δt_c, against initial relative velocity, v_i, for the large glass beads with the parameters used for Figure 4 and $c_1 = c_2 = c_3$ values of 0, 100 and 200 $\mathrm{kg\,s^{-1}}$.

5. A NOTE ON LINEAR STABILITY

In this section, we will show that linearisation alone cannot be applied to aid in the analytical development of time-step criteria for nonlinear systems. The system given by (45) – (50) can be

Prepared using nmeauth.cls
DOI: 10.1002/nme

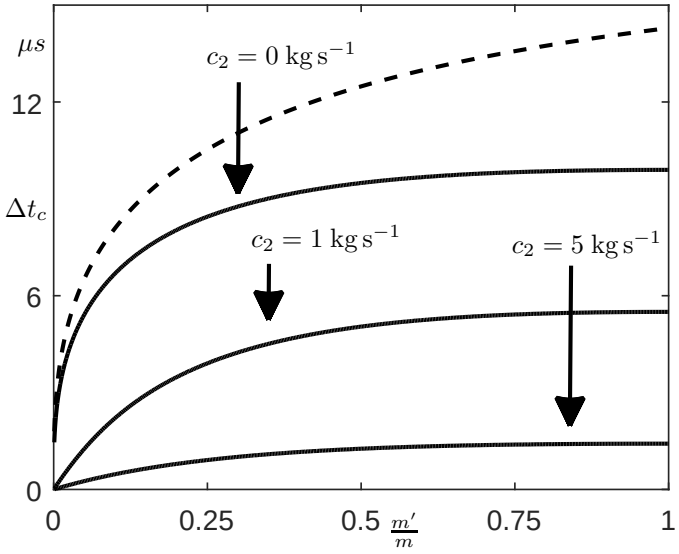

Figure 11. Critical time-step, Δt_c, against particle mass ratio, $\frac{m'}{m}$, for an industrial powder with the parameters used for Figure 5, v_i = 1 m s^{-1} and $c_1 = c_2 = c_3$ values of 0, 1 and 5 kg s^{-1}.

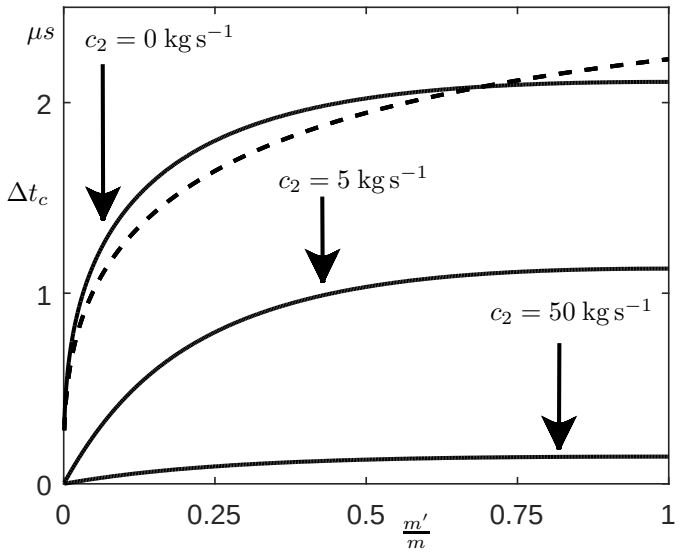

Figure 12. Critical time-step, Δt_c, against particle mass ratio, $\frac{m'}{m}$, for glass ballotini with the parameters used for Figure 6, v_i = 1 m s^{-1} and $c_1 = c_2 = c_3$ values of 0, 5 and 50 kg s^{-1}.

viewed as a discrete nonlinear map. It is therefore intuitive to employ dynamical systems theory to complement the time-step stability analysis.

Prepared using nmeauth.cls
DOI: 10.1002/nme

5.1. *Fixed Points*

Fixed points of a *discrete dynamical system*, or a *map*, can be viewed as a static value of the *dynamical system* or constant solutions to the discrete equations. Consider the j-dimensional map

$$x_{n+1} = f\left(x_n\right), \tag{79}$$

where $x = (x_1, \ldots, x_j)^T$ and $f(x) = (f_1, \ldots, f_j)^T$ is a function of the system variable x, such that

$$x_{1\,n+1} = f_1\left(x_{1\,n}, \ldots, x_{j\,n}\right) \tag{80}$$

$$\vdots$$

$$x_{j\,n+1} = f_j\left(x_{1\,n}, \ldots, x_{j\,n}\right) \tag{81}$$

Any fixed point $x^* = ({x_1}^*, \ldots {x_j}^*)^T$ of the map (80) – (81) must satisfy the equations

$$f_1\left({x_1}^*, \ldots {x_j}^*\right) = {x_1}^*, \quad \cdots, \quad f_j\left({x_1}^*, \ldots {x_j}^*\right) = {x_j}^*. \tag{82}$$

Solutions of (82) give us the location of the fixed points and, potentially, also some insight into the stability characteristics of the nonlinear system.

5.2. *Stability of the linearised systems*

In order to ascertain the linear stability characteristics of a fixed point of a nonlinear map, it is necessary to consider a linearisation of the map in the neighborhood of the fixed point. This can be achieved by computing the Jacobian $J(x^*)$ of the nonlinear map evaluated at the fixed point, and thus we end up with a linear map given by

$$x_{n+1} = J(x^*)x_n, \tag{83}$$

that is valid in the vicinity of x^*. For the map (80) – (81) we have the linear system

$$\begin{pmatrix} x_{1\,n+1} \\ \vdots \\ x_{j\,n+1} \end{pmatrix} \approxeq \begin{pmatrix} \frac{\partial f_1}{\partial x_1}\left({x_1}^*, \ldots, {x_j}^*\right) & \cdots & \frac{\partial f_1}{\partial x_j}\left({x_1}^*, \ldots, {x_j}^*\right) \\ \vdots & \ddots & \vdots \\ \frac{\partial f_j}{\partial x_1}\left({x_1}^*, \ldots {x_j}^*\right) & \cdots & \frac{\partial f_j}{\partial x_j}\left({x_1}^*, \ldots, {x_j}^*\right) \end{pmatrix} \begin{pmatrix} x_{1\,n} \\ \vdots \\ x_{j\,n} \end{pmatrix}, \tag{84}$$

which is linearised about the fixed point $x^* = ({x_1}^*, \ldots {x_j}^*)^T$.

Prepared using nmeauth.cls
DOI: 10.1002/nme

The linear stability of the fixed point is determined by the nature of the eigenvalues λ_i of the Jacobian evaluated at the fixed point. In general, a fixed point is asymptotically stable if all eigenvalues are contained within the unit circle of the complex plane, i.e., such that $|\lambda_i| < 1$; otherwise the fixed point is unstable.

5.3. *Reduced dynamics*

If we consider the reduced system and the dynamics in the normal direction only, the map given by (45) – (50) reduces to

$$\hat{v}_{n+1} = \hat{v}_n - \Delta t \left(\frac{k_2}{\hat{m}} x_n{}^{\frac{3}{2}} + \frac{c_2}{\hat{m}} \hat{v}_n \right), \tag{85}$$

$$x_{n+1} = x_n + \Delta t \hat{v}_{n+1}. \tag{86}$$

Using (82), we find that the only fixed point for the reduced map is $(v^*, x^*)^T = (0,0)^T$. The linearised system about $(v, x) = (0,0)^T$ can then be found, using (84), and is given by

$$\begin{pmatrix} \hat{v}_{n+1} \\ x_{n+1} \end{pmatrix} = \begin{pmatrix} 1 - \frac{c_2 \Delta t}{\hat{m}} & 0 \\ \Delta t - \frac{c_2 \Delta t^2}{\hat{m}} & 1 \end{pmatrix} \begin{pmatrix} \hat{v}_n \\ x_n \end{pmatrix}. \tag{87}$$

The Jacobian of the linearised system, evaluated at the fixed point, has the eigenvalues

$$\lambda_1 = 1, \quad \lambda_2 = 1 - \frac{c_2 \Delta t}{\hat{m}} \tag{88}$$

with corresponding eigenvectors

$$v_1 = \begin{pmatrix} 0 \\ 1 \end{pmatrix}, \quad v_2 = \begin{pmatrix} \frac{c_2}{c_2 \Delta t - \hat{m}} \\ 1 \end{pmatrix}. \tag{89}$$

Since one of the eigenvalues is equal to 1, we have that the fixed point in this setup is degenerate and thus the local dynamics are given by one (stable or unstable) manifold and a centre manifold. Furthermore, as mentioned above, the stability of the fixed point requires that the second manifold is stable and thus λ_2 has to be contained within the unit circle of the complex plane, such that $|\lambda_2| \leq 1$. Applying this criterion to λ_2 given in (88) gives

$$0 \leq \Delta t \leq \frac{2\hat{m}}{c_2}. \tag{90}$$

Prepared using nmeauth.cls
DOI: 10.1002/nme

This analysis only holds, however, for the flow in the vicinity of the fixed point. For a sufficiently small initial relative velocity, this would be an appropriate bound on the time-step. This bound is independent of the spring force, and is more than twice the value calculated in (65), derived for the unloading from maximum compression to separation (Phase 2).

Linearisation is the most commonly used tool for analysing the stability of nonlinear systems in engineering. This analysis clearly shows that one should be very careful when linearising and using that as an approximation of what happens in the systems. This further motivates the need for a new method for selecting stable time steps for nonlinear systems. To really understand what happens locally to the fixed point would require further analysis and lies outside the scope of the present analysis.

6. DISCUSSION AND CONCLUSIONS

An alternative technique has been proposed to determine numerical simulation stability for a nonlinear contact interaction including damping, based on analysing the dynamics of the impact phase. This method is based on a general framework which analyses the contact phase in terms of the discretised contact point equations of motion which form a linear or nonlinear map (depending on the nature of the contact law). This general framework is compatible for collisions of spherical particles subject to a linear or nonlinear contact law.

We performed a numerical investigation of how the critical time-step varies as a function of the system damping together with the initial relative velocity of collision. This analysis is the first of its kind and provides an intuitive, easy-to-use technique for engineers who want to ensure stable, but not overly conservative, numerical simulations of dynamic systems with damping. The analytical and numerical results presented here have also confirmed previous observations in the literature showing how the numerics become less stable with increased system damping and relative collision velocity.

This analysis is only applicable to two contacting spherical particles, as is the case for the commonly used Rayleigh time-step approach. Nevertheless, it still provides a very useful guide for

Prepared using nmeauth.cls
DOI: 10.1002/nme

how to choose a stable time-step for dynamic systems with damping. Furthermore, the framework presented here is general so can be extended, e.g., to incorporate a close-packing of spherical particles, a configuration more representative of certain DEM use cases. Pending such a study, it is important to note that Δt_c should be reduced for multiple inter-particle contacts. Recently, Otsubo et al. [11] discovered the relationship $\Delta t_c \propto C_{N,\max}^{-\frac{2}{3}}$ for a specific polydisperse packing of spheres with a Hertz–Mindlin contact model where $C_{N,\max}$ is the maximum particle coordination number.

A basic introduction to dynamical systems theory was given and used to determine the stability of a simplified version of the model system for low-velocity collision cases. While the results are only partial, it shows that linearisation alone does not give us all the answers to the stability of the full system. However, the proportionality of the stability bound to $\frac{\hat{m}}{c_2}$ obtained further confirms the validity of the bound for the unloading phase of the inter-particle impact. The extension of this work has been left to future research.

In practice, a safety factor is included when using the Rayleigh time-step. We propose using a similar safety factor for the implementation of our critical time-step. The safety factor can be viewed as the approximate number of steps required to accurately describe the individual segments of the impact phase. From the numerical results, we have found that our critical time-step exceeds the Rayleigh time-step for a large region of parameter space. Arguably more important, however, is the fact that we have highlighted the regions in parameter space where a much more conservative time-step is required. This further emphasizes the shortcomings of the Rayleigh time-step approach.

ACKNOWLEDGEMENTS

This work was supported by the EPSRC grant EP/N004477/1. We thank Mark Cook, Andreas Piskopakis and Marina Sousani from DEM Solutions for their useful comments. We also thank Di Peng at the University of Edinburgh for his comments on drafts of this paper.

References

Prepared using nmeauth.cls
DOI: 10.1002/nme

1. Cundall PA, Strack ODL. A discrete numerical model for granular assemblies. *Géotechnique* 1979; **29**(1):47–65.
2. Rougier E, Munjiza A, John NWM. Numerical comparison of some explicit time integration schemes used in DEM, FEM/DEM and molecular dynamics. *International Journal for Numerical Methods in Engineering* 2004; **61**:856–879.
3. Bathe KJ, Wilson EJ. *Numerical methods in finite element analysis*. Prentice Hall, INC, New Jersey, 1976.
4. Burns SJ, Hanley KJ. Establishing stable time-steps for DEM simulations of non-collinear planar collisions with linear contact laws. *International Journal for Numerical Methods in Engineering* 2017; **110**(2):186–200.
5. Belytschko T, Liu WK, Moran B, Elkhodary KI. *Nonlinear finite elements for continua and structures*. 2 edn., Wiley, New York, 2013.
6. O'Sullivan C. *Particulate discrete element modelling: A geomechanics perspective*. 1 edn., Taylor & Francis, UK, 2011.
7. Belytschko T. *An overview of semidiscretization and time integration procedures, in Belytschko, T. and Hughes, T. J. R, (Eds), Computational methods for Transient Analysis, Computational Methods in Mechanics Series*. North Holland, New York, 1983.
8. Wood WL. *Practical time-stepping schemes*. Oxford: Clarendon Press, 1990.
9. Hart R, Cundall PA, Lemos J. Formulation of a three-dimensional distinct element modelpart ii. mechanical calculations for motion and interaction of a system composed of many polyhedral blocks. *International Journal of Rock Mechanics and Mining Sciences & Geomechanics Abstracts* 1988; **25**(3):117–125.
10. Han K, Perić D, Owen DRJ, Yu J. A combined finite/discrete element simulation of shot peening processes – Part II: 3D interaction laws. *Engineering Computations* 2000; **17**(6):680–702.
11. Otsubo M, O'Sullivan C, Shire T. Empirical assessment of the critical time increment in explicit particulate discrete element method simulations. *Computers and Geotechnics* 2017; **86**:67–79.
12. Wada K, Senshu H, Matsui T. Numerical simulation of impact cratering on granular material. *Icarus* 2006; **180**(2):528–545.
13. Timoshenko SP, Goodier JN. *Theory of Elasticity*. 3 edn., McGraw-Hill, 1970.
14. Tsuji Y, Kawaguchi T, Tanaka T. Discrete particle simulation of two-dimensional fluidized bed. *Powder Technology* 1993; **77**(1):79–87.
15. Rojek J, Nosewicz S, Jurczak K, Chmielewski M, Bochenek K, Pietrzak K. Discrete element simulation of powder compaction in cold uniaxial pressing with low pressure. *Computational Particle Mechanics* 2016; **3**(4):513–524.
16. Tu X, Andrade JE. Criteria for static equilibrium in particulate mechanics computations. *International Journal for Numerical Methods in Engineering* 2008; **75**(13):1581–1606.
17. O'Sullivan C, Bray JD. Selecting a suitable timestep for discrete element simulations that use the central difference algorithm time integration scheme. *Engineering Computations* 2004; **21**(2/3/4):278–303.
18. Livermore Software Technology Corporation. *LS-DYNA Theory Manual*. Livermore Software Technology Corporation, Livermore, California, 2006.
19. ABAQUS, Inc. *ABAQUS Theory Manual (v6.6)*. ABAQUS, Inc., Providence, Rhode Island, 2006.

Prepared using nmeauth.cls
DOI: 10.1002/nme

20. Li Y, Xu Y, Thornton C. A comparison of discrete element simulations and experiments for ‘sandpiles’ composed of spherical particles. *Powder Technology* 2005; **160**(3):219–228.
21. Johnson KL. *Contact mechanics*. Springer, 1985.
22. Thornton C, Randall CW. *Applications of theoretical contact mechanics to solid particle system simulation, in Satake, M. and Jenkins, J. T., (Eds), Micromechanics of Granular Materials*. Elsevier, 1988.
23. Kremmer M, Favier JF. A method for representing boundaries in discrete element modelling – part II: Kinematics. *International Journal for Numerical Methods in Engineering* 2001; **51**(12):1423–1436.
24. Kafui KD, Thornton C, Adams MJ. Discrete particle-continuum fluid modelling of gas–solid fluidised beds. *Chemical Engineering Science* 2002; **57**(13):2395–2410.
25. Itasca Consulting Group. *PFC3D: Particle Flow Code in Three Dimensions User’s Guide*. 4 edn., Itasca Consulting Group, Minneapolis, Minnesota, 2008.
26. Hanley KJ, O’Sullivan C. Analytical study of the accuracy of discrete element simulations. *International Journal for Numerical Methods in Engineering* 2017; **109**(1):29–51.
27. Chung Y, OOi J. Benchmark tests for verifying discrete element modelling codesat particle impact level. *Grannular Matter* 2011; **13**:643–656.
28. Goldsmith W. *Impact: The theory and physical behaviour of colliding solids*. Dover Publications, 2001.
29. Gao Y, Boukouvala F, Engisch W, Meng W, Muzzio FJ, Ierapetritou MG. Improving continuous powder blending performance using projection to latent structures regression. *Journal of Pharmaceutical Innovation* 2013; **8**(2):99–110.
30. Chung YC, Ooi JY. Influence of discrete element model parameters on bulk behavior of a granular solid under confined compression. *Particulate Science and Technology* 2007; **26**(1):83–96.
31. Washino K, Chan EL, Miyazaki K, Tsuji T, Tanaka T. Time step criteria in DEM simulation of wet particles in viscosity dominant systems. *Powder Technology* 2016; **302**:100–107.

Prepared using nmeauth.cls
DOI: 10.1002/nme